

Article

Random Material Property Fields of 3D Concrete Microstructures Based on CT Image Reconstruction

George Stefanou ^{*}, Dimitrios Savvas and Panagiotis Metsis

Department of Civil Engineering, Institute of Structural Analysis & Dynamics of Structures, Aristotle University of Thessaloniki, 54124 Thessaloniki, Greece; dimitriosavvas@yahoo.gr (D.S.); panos@metsis.gr (P.M.)

* Correspondence: gstefanou@civil.auth.gr

Abstract: The purpose of this paper is to determine the random spatially varying elastic properties of concrete at various scales taking into account its highly heterogeneous microstructure. The reconstruction of concrete microstructure is based on computed tomography (CT) images of a cubic concrete specimen. The variability of the local volume fraction of the constituents (pores, cement paste and aggregates) is quantified and mesoscale random fields of the elasticity tensor are computed from a number of statistical volume elements obtained by applying the moving window method on the specimen along with computational homogenization. Based on the statistical characteristics of the mesoscale random fields, it is possible to assess the effect of randomness in microstructure on the mechanical behavior of concrete.

Keywords: concrete; CT images; reconstruction; 3D FE models; homogenization; mesoscale random fields



Citation: Stefanou, G.; Savvas, D.; Metsis, P. Random Material Property Fields of 3D Concrete Microstructures Based on CT Image Reconstruction. *Materials* **2021**, *14*, 1423. <https://doi.org/10.3390/ma14061423>

Academic Editor: Jean-Marc Tulliani

Received: 2 February 2021

Accepted: 8 March 2021

Published: 15 March 2021

Publisher's Note: MDPI stays neutral with regard to jurisdictional claims in published maps and institutional affiliations.



Copyright: © 2021 by the authors. Licensee MDPI, Basel, Switzerland. This article is an open access article distributed under the terms and conditions of the Creative Commons Attribution (CC BY) license (<https://creativecommons.org/licenses/by/4.0/>).

1. Introduction

The macroscopic mechanical properties of heterogeneous materials consisting of multiple phases such as particle-reinforced composites and concrete are significantly influenced by their underlying microstructure and can be determined through numerical homogenization. The application of homogenization methods in the analysis of multi-phase materials offers an efficient alternative over direct simulation of the microstructure in terms of required computational resources. The key issue in homogenization methods is the linking of micromechanical characteristics with the random variation of material properties at higher scales, which is usually established using Hill's macro-homogeneity condition [1]. In this framework, it is necessary to identify a representative volume element (RVE) usually through computational convergence schemes with respect to specific apparent properties [2]. In contrast to the RVE, which is characterized by deterministic material properties, the spatial variation of the elasticity tensor at lower scales is quantified by random fields computed on mesoscale models—statistical volume elements (SVEs) [3,4].

The highly heterogeneous microstructure of concrete is responsible for its complex mechanical behavior. Therefore a wide variety of methods have been developed for the accurate reconstruction of concrete microstructure mostly based on image processing and random fields. The geometrical characteristics of aggregates are statistically analyzed in [5] by processing 2D images of concrete obtained from X-ray computed tomography (CT). A recent review on the use of micro-CT images to investigate the relation between microstructural features and properties of cement-based materials is provided in [6] showing the important role of threshold determination on phase identification. Two non-Gaussian random field models are developed in [7] for simulating the geometry of star-like inclusions in heterogeneous materials. For illustration, the models are calibrated to the geometrical features of a population of aggregates used in concrete. Huang and Peng [8] present a multiscale computational framework for generating concrete microstructures by concurrently

coupling stationary Gaussian and fractional Brownian random fields, used to simulate coarse and fine aggregates, respectively.

The mechanical properties of concrete are determined using computational homogenization in a number of publications. Constantinides and Ulm [9] confirm the existence of two types of calcium-silicate-hydrate (C-S-H) in cement-based materials, and examine the effect of the two phases on the Young's modulus and Poisson ratio of this kind of material by means of nanoindentation tests. The effective properties of cement pastes are computed using a homogenization model based on the elastic properties and volume fractions of the two phases. Wriggers and Moftah [10] generate 3D concrete microstructures taking into consideration the random aggregate morphology at the mesoscale. Then the finite element (FE) method is used for the homogenization of concrete. In [11], 2D and 3D homogenization and fracture analysis of concrete are performed based on micro-CT images and Monte Carlo simulation. Tal and Fish [12] determine a realistic RVE of concrete, which represents its random microstructure. A probabilistic upscaling procedure for modeling the mesoscale elastic properties of concrete at the level of SVE is provided by Dubey and Noshadravan [13]. To the authors' knowledge, the random spatial variability of the mechanical properties of concrete at various scales has not been thoroughly investigated yet.

The purpose of the present paper is to provide a complete probabilistic description of the spatial variation of the elastic properties of concrete taking into account its highly heterogeneous microstructure, which is reconstructed using CT images of a cubic concrete specimen. The variability of local volume fraction of the constituents (pores, cement paste and aggregates) is quantified first. Mesoscale random fields of the elasticity tensor are computed subsequently from a number of SVEs obtained by applying the moving window method on the concrete specimen along with computational homogenization. Based on the statistical features (empirical distribution and correlation functions) of the random fields, it is possible to assess the effect of randomness in microstructure on the mechanical behavior of concrete.

The paper is organized as follows: In Section 2, the process of reconstructing concrete microstructure based on CT images is described. Section 3 presents the framework of computational homogenization used to determine the random spatially varying apparent elasticity tensor of 3D concrete microstructures. The numerical results obtained using the proposed approach are discussed in the next section followed by some concluding remarks in Section 5.

2. Reconstruction of Concrete Microstructure Based on CT Images

2.1. CT Images

Computed Tomography (CT) has its origins in the medical field and refers to a computerized X-ray imaging procedure in which a patient is struck by a narrow X-ray beam that rotates at a certain speed around the patient's body. While the CT procedure has been applied mainly for medical purposes, the gradual increase in available CT equipment and the improvement of the cost factors have led to other utilizations, such as the exploration of the microstructure of heterogeneous materials [14]. When the X-ray beam passes through a sample, some of the X-ray radiation is absorbed and scattered, while the rest penetrates through the sample, as shown in Figure 1.

The absorbed or scattered radiation of a material can be measured in Hounsfield units (HU). HU is a quantitative scale that reflects the linear transformation of the original linear attenuation coefficient measurement (μ) so as the radiodensity of distilled water at standard pressure and temperature is defined as zero HU, while the radiodensity of air, at the same conditions, is defined as -1000 HU. The linear transformation used to convert the attenuation values μ to HU values on each pixel of the CT image is as follows:

$$HU = \mu \times slope + intercept \quad (1)$$

where the values of the rescale slope and intercept parameter are specific to the CT scanner system used [15,16]. Their values can be obtained from the extracted DICOM (Digital Imaging and Communications in Medicine) files.

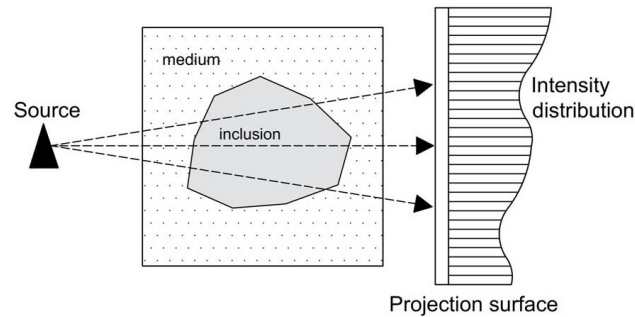


Figure 1. Intensity Distribution of an X-ray array.

2.2. Reconstruction of Concrete Microstructure

The reconstruction of concrete microstructure is based on data obtained from the CT scan. The specimen is cut in 2D slices (images) with their corresponding resolution (Figure 2). Each pixel carries, beside its geometric properties, the attenuation value μ that is converted to the respective HU value using Equation (1). Then, by utilizing voxels (the generalization of pixels on a regularly spaced, three-dimensional grid), the voxel-based FE method is employed. Using the moving window technique [17], random mesoscale models or SVEs are created, which are discretized by a structured FE mesh based on voxels geometry.

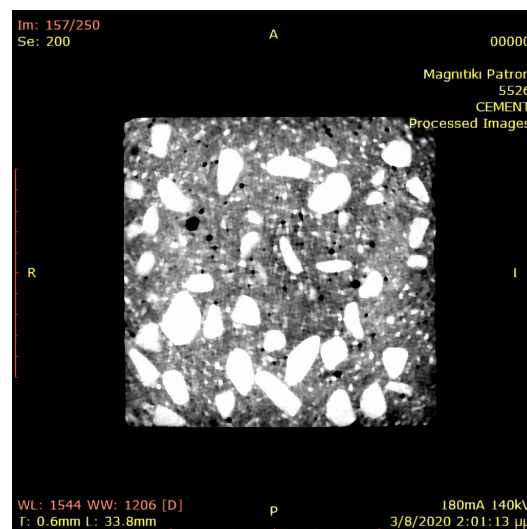


Figure 2. A 2D computed tomography (CT) image of concrete.

In this work, the medical CT scan was conducted at the laboratory of Magnitiki Patron S.A. [18], which has provided all the DICOM data for the reconstruction of concrete microstructure. The equipment used was a LightSpeed VCT of GE Medical Systems Hellas (Athens, Greece) with peak potential and current applied to the X-ray tube equal to 140 kV and 180 mA, respectively. The axial resolution of the scan was fixed at 0.625 mm resulting in 211 total slices, while the pixel resolution of the 2D image in each slice plane is $0.4883 \times 0.4883 \text{ mm}^2$, resulting in 281×281 pixels. Note that the dimensions of the scanned cubic concrete specimen was approximately $136.724 \times 136.724 \times 131.25 \text{ mm}^3$. For the visualization of the image data the RadiAnt DICOM viewer software [19] has been used.

3. Computational Homogenization

A fundamental assumption in the homogenization process is the statistical homogeneity of the heterogeneous medium [20]. This means that, at any material point of the medium all statistical properties of the state variables are the same and thus identification of the RVE is possible. In case of composites with periodic or nearly periodic geometry, the RVE is explicitly defined [21] whereas in case of spatial randomness, the RVE needs to be determined using computational methods [3,22–27].

A basic principle for the existence of the RVE is separation of scales as defined below [1]:

$$d \ll L \ll L_{macro} \quad (2)$$

where the microscale parameter d denotes a characteristic size of the fillers, e.g., the average dimension of aggregates, the mesoscale parameter L denotes the size of the volume element and the macroscale parameter L_{macro} denotes the characteristic length over which the macroscopic loading varies in space. Note that, in the case of complete scale separation, L_{macro} denotes the size of the macroscopic homogeneous medium.

The statistical characteristics of the apparent elasticity tensor of concrete are computed by analyzing a set of random mesoscale models or SVEs. These are obtained by applying the moving window technique on a cubic concrete specimen reconstructed based on a set of 2D CT images (see Section 2). Figure 3 depicts the cubic concrete specimen segmented into a large number of non-overlapping SVEs along with a detail of the voxel based FE mesh of a specific SVE. Each SVE model is characterized by the scale factor $\delta = L/d$, which is a non-dimensional parameter with $\delta \in [1, \infty]$. The length scale of the SVE is always smaller than the one of the corresponding RVE. For each positioning of the moving window, the apparent material properties are computed through homogenization. The obtained mesoscale properties and corresponding window centres are used to form the related random field model, as shown in Section 4.

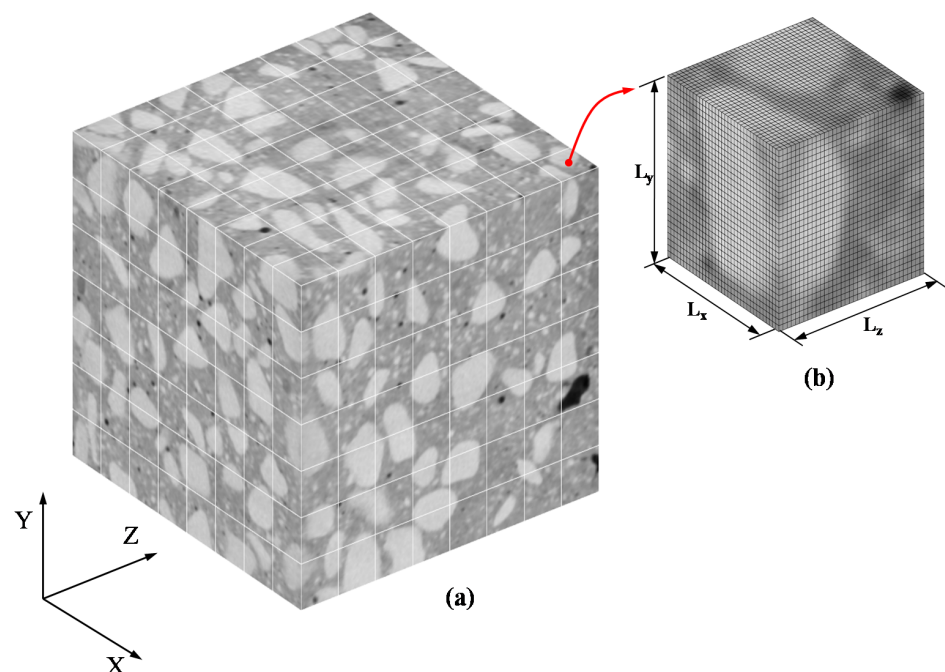


Figure 3. (a) Schematic of 3D moving window technique on a cubic concrete specimen reconstructed using 2D CT images, (b) Detail of the voxel based finite element (FE) mesh of a specific statistical volume element (SVE) model of dimensions $L_x \times L_y \times L_z$.

$$\bar{\varepsilon} = \left\{ \begin{array}{l} \left[\begin{array}{c} \bar{\varepsilon}_{11} = 1 \\ 0 \\ 0 \\ 0 \\ 0 \\ 0 \end{array} \right], \left[\begin{array}{c} 0 \\ \bar{\varepsilon}_{22} = 1 \\ 0 \\ 0 \\ 0 \\ 0 \end{array} \right], \left[\begin{array}{c} 0 \\ 0 \\ \bar{\varepsilon}_{33} = 1 \\ 0 \\ 0 \\ 0 \end{array} \right], \left[\begin{array}{c} 0 \\ 0 \\ 0 \\ \bar{\varepsilon}_{12} = 1 \\ 0 \\ 0 \end{array} \right], \left[\begin{array}{c} 0 \\ 0 \\ 0 \\ 0 \\ \bar{\varepsilon}_{23} = 1 \\ 0 \end{array} \right], \left[\begin{array}{c} 0 \\ 0 \\ 0 \\ 0 \\ 0 \\ \bar{\varepsilon}_{31} = 1 \end{array} \right] \end{array} \right\} \quad (9)$$

The imposed displacements on the boundary nodes of each SVE are calculated through the prescribed uniform strain tensor using the following equation:

$$\mathbf{u}_b = D_b^T \bar{\varepsilon} \quad (10)$$

where the geometric matrix D_b is calculated for a boundary node b based on its coordinates:

$$D_b = \frac{1}{2} \begin{bmatrix} 2x_b & 0 & 0 \\ 0 & 2y_b & 0 \\ 0 & 0 & 2z_b \\ y_b & x_b & 0 \\ 0 & z_b & y_b \\ z_b & 0 & x_b \end{bmatrix} \quad \text{with } (x_b, y_b, z_b) \in \mathbf{x} \quad (11)$$

The BVP which has to be solved is as follows:

$$\begin{bmatrix} \mathbf{K}_{ii} & \mathbf{K}_{ib} \\ \mathbf{K}_{bi} & \mathbf{K}_{bb} \end{bmatrix} \begin{bmatrix} \mathbf{u}_i \\ \mathbf{u}_b \end{bmatrix} = \begin{bmatrix} \mathbf{f}_i \\ \mathbf{f}_b \end{bmatrix} \quad (12)$$

where the stiffness matrix \mathbf{K} of the FE model is rearranged into four sub-matrices associated with interior nodes i and boundary nodes b . The macroscopic stress tensor is then calculated as a volume average by:

$$\bar{\sigma} = \frac{1}{V} \mathbb{D} \mathbf{f}_b \quad (13)$$

where $\mathbf{f}_b = \mathbf{K}_{bb} \mathbf{u}_b + \mathbf{K}_{bi} \mathbf{u}_i$ is the vector containing the computed reaction forces on the boundary nodes, $\mathbf{u}_i = \mathbf{K}_{ii}^{-1} (\mathbf{f}_i - \mathbf{K}_{ib} \mathbf{u}_b)$ is the vector containing the calculated displacements of the interior nodes and $\mathbb{D} = [D_1 \ D_2 \ \dots \ D_{n_b}]$ with n_b the total number of boundary nodes b .

4. Numerical Results and Discussion

In this section, numerical results concerning the determination of the random fields, the empirical distributions and the 3D spatial correlations of the components of the homogenized elasticity tensor of the 3D concrete specimen are presented for various scale factors δ examined. As shown in Figure 3, the size of each SVE corresponds to that of the selected 3D window in the moving window technique. Moreover, the moving window step in each direction has been selected equal to the size of the examined window so as non-overlapping SVEs are extracted. In the following parametric study the examined mesoscale sizes δ_i with $i = 1, 2, 3, 4$, correspond to different window sizes and thus different total numbers of SVEs (see Table 1).

Table 1. Size of window and total number of SVEs corresponding to each δ_i examined.

δ_i	$L_x \times L_y \times L_z$ (mm ³)	No. SVEs
δ_1	$4.88 \times 4.88 \times 6.25$	16,464
δ_2	$9.77 \times 9.77 \times 8.75$	2940
δ_3	$19.53 \times 19.53 \times 18.75$	343
δ_4	$27.34 \times 27.34 \times 26.25$	125

In the context of FE simulation, the discretization of the SVEs into hexahedral solid elements is based on the voxels which are used to reconstruct the 3D geometry of the

concrete specimen. Information about the pixels (e.g., location, spacing, attenuation values μ) and the slices (e.g., position, thickness) needed in order to construct the voxels and also to identify the constituent materials is included in the DICOM files provided by the CT scan system. In order to reduce the required computational cost, each hexahedral solid element in the FE mesh of the SVEs corresponds to $2 \times 2 \times 2$ voxels. The material assigned to each integration point of an element depends on the HU value of the integration point which is calculated by interpolating the nodal HU values using the shape functions of the element.

Figure 4 depicts the histogram (empirical distribution) of the Hounsfield units (HU) calculated by Equation (1) with rescale slope and rescale intercept equal to 1 and -1024 , respectively, for the CT equipment used. From this figure, the constituent materials (pores, cement and aggregates) can be distinguished by defining specific ranges for their HU values. Based on the observed peaks of the histogram and after careful processing of the CT images using RadiAnt DICOM viewer, the HU range can be selected as $[-960, 800]$ for pores, $[800, 2000]$ for cement and $[2000, 2974]$ for aggregates. Figure 4 depicts also a gray scale colorbar related to the HU values of the constituent materials of concrete. The illustration of concrete specimen in Figure 3 is based on this color range.

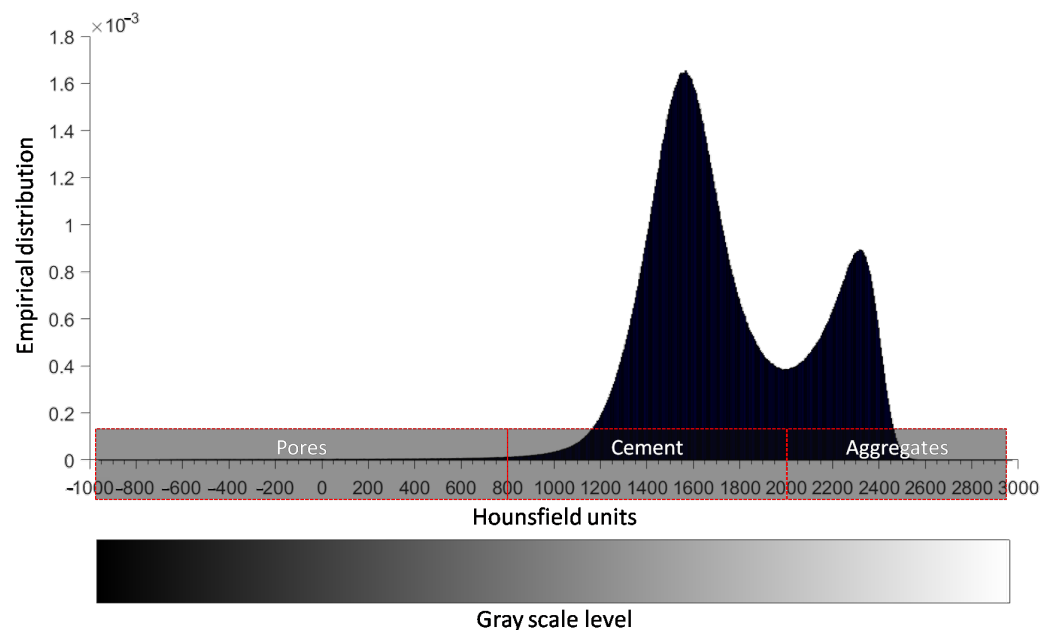


Figure 4. Empirical distribution of Hounsfield unit (HU) values derived from all CT images followed by the range of HU for concrete constituent materials.

Based on the aforementioned HU ranges, the local volume fraction (vf) variability of the constituents of concrete can be studied next. Figure 5 illustrates the computed 3D random fields along with the respective empirical distributions of the volume fraction of the constituent materials for δ_1 . The dispersion of aggregates within cement paste is not uniform and also, some air was trapped inside the paste during the mixture process. These facts are evident in Figure 5, where regions of material rich or poor in aggregates and pores can be observed. The mean vf of the constituents in the concrete specimen is 0.5% pores, 72.3% cement and 27.2% aggregates. For visualization purposes, Figures 5–7 provide 2D contour plots of the random fields corresponding to the three orthogonal planes (XY, YZ and ZX) intersected at the center point of the cubic concrete specimen.

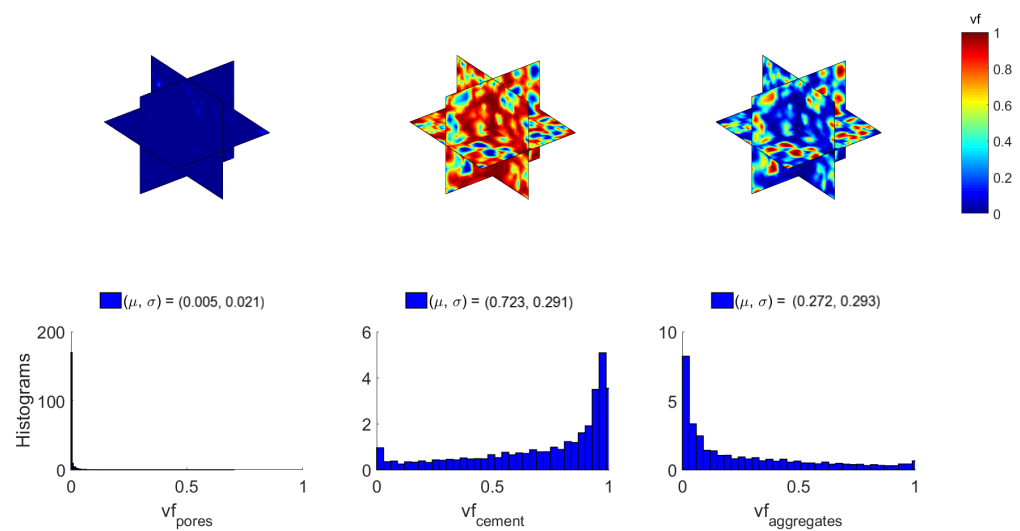


Figure 5. Random fields and histograms of volume fraction (vf) of concrete constituents for δ_1 .

Figures 6 and 7 illustrate the computed random fields and the empirical distributions of the apparent \bar{C}_{11} (axial) and \bar{C}_{44} (shear) stiffness with respect to δ_i (see Equation (8) with correspondence of subscripts: $1 \rightarrow 11$ and $4 \rightarrow 12$). These results have been obtained by implementing the homogenization method presented in Section 3 in each mesoscale size δ_i . The constituent materials of concrete are considered linear elastic. Specifically, their Young's modulus and Poisson ratio $[E, \nu]$ are assumed as $[20 \text{ GPa}, 0.2]$ for cement and $[100 \text{ GPa}, 0.2]$ for aggregates. Note that pores can be modeled by setting their Young's modulus equal to 0.2 GPa (1% of the Young's modulus of cement) and Poisson ratio equal to 0.45 (almost incompressible material). From Figures 6 and 7, it can be observed that random fields become less variable and histograms narrow as the scale factor δ increases. Specifically, the coefficient of variation (COV) reduces from 63% to 17% for both \bar{C}_{11} and \bar{C}_{44} as δ increases. However, it is deduced that morphological uncertainty can lead to significant random spatial variation of the mechanical properties of concrete.

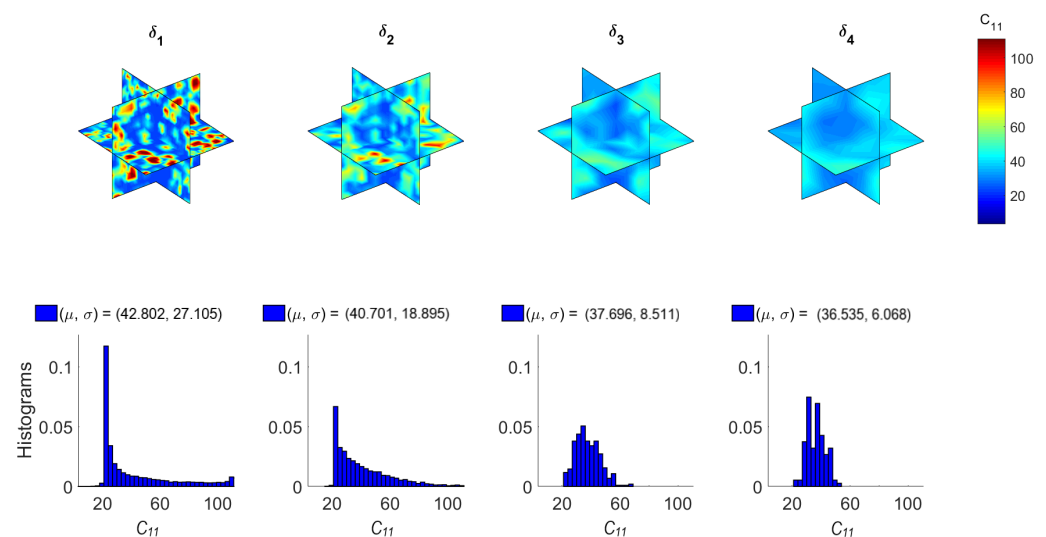


Figure 6. Random fields and histograms of \bar{C}_{11} .

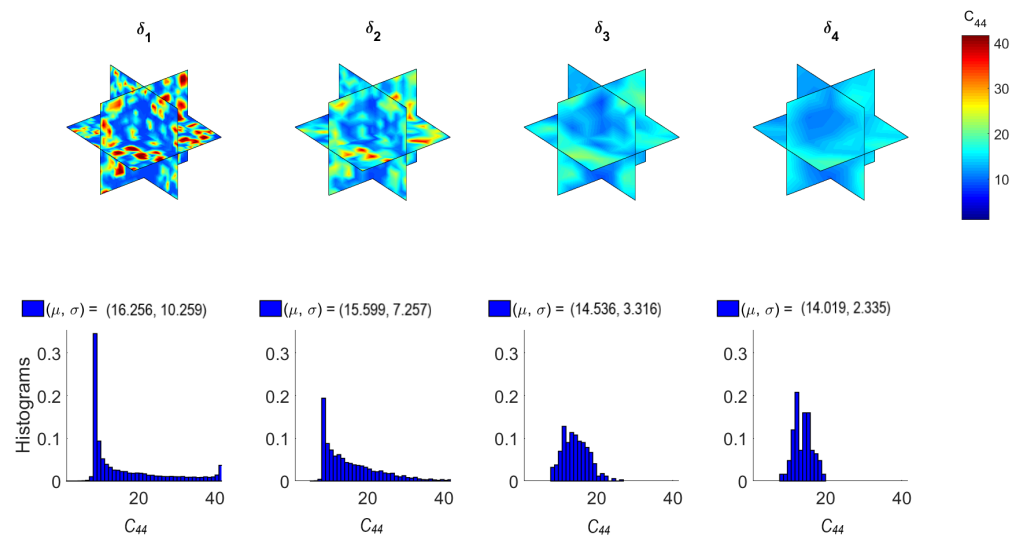


Figure 7. Random fields and histograms of \bar{C}_{44} .

Figures 8–10 depict the 3D spatial correlations of $\hat{\rho}_{\bar{C}_{11}}^{\bar{C}_{11}}$, $\hat{\rho}_{\bar{C}_{44}}^{\bar{C}_{44}}$ and $\hat{\rho}_{\bar{C}_{11}}^{\text{vf}_{\text{aggr}}}$, respectively, for increasing mesoscale size δ_i . For visualization purposes, the aforementioned figures depict the spatial correlation values corresponding to the three orthogonal planes (XY, YZ and ZX) intersected at the center point of the cubic concrete specimen. The estimates of the spatial correlation functions $\hat{\rho}_A^B$ have been calculated for every lag (ξ_x, ξ_y, ξ_z) according to the following formula:

$$\hat{\rho}_A^B(\xi_x, \xi_y, \xi_z) = \frac{1}{n-1} \sum_{i=0}^{n_{wx}} \sum_{j=0}^{n_{wy}} \sum_{k=0}^{n_{wz}} \left(\frac{A(x^i, y^j, z^k) - \hat{\mu}_A}{\hat{\sigma}_A} \right) \left(\frac{B(x^i + \xi_x, y^j + \xi_y, z^k + \xi_z) - \hat{\mu}_B}{\hat{\sigma}_B} \right) \quad (14)$$

$$-n_{wx}\Delta\xi_x \leq \xi_x \leq n_{wx}\Delta\xi_x, \quad -n_{wy}\Delta\xi_y \leq \xi_y \leq n_{wy}\Delta\xi_y, \quad -n_{wz}\Delta\xi_z \leq \xi_z \leq n_{wz}\Delta\xi_z$$

with $\hat{\rho}_A^B$ denoting auto-correlations when $A \equiv B$, otherwise cross-correlations are defined. $\hat{\mu}_A, \hat{\mu}_B$ are the sample mean values while $\hat{\sigma}_A, \hat{\sigma}_B$ are the sample standard deviations of quantities A, B , respectively. The total number of SVEs is $n = n_{wx}n_{wy}n_{wz}$. It can be observed that the correlation length of all mesoscale random fields increases as the scale factor δ increases. In other words, the random fields become fully correlated for large δ [30]. The auto-correlations for lag $(\xi_x = 0, \xi_y = 0, \xi_z = 0)$ are 1 and tend to zero for lag values $|\xi_x| > L_x, |\xi_y| > L_y$ and $|\xi_z| > L_z$. The cross-correlations have similar behavior with maximum value at zero lag less than 1. This can be attributed to the fact that the probability of SVEs to share common aggregates is decreased as the length of the vector $\vec{\xi}_p = [\xi_x, \xi_y, \xi_z]$ is increased.

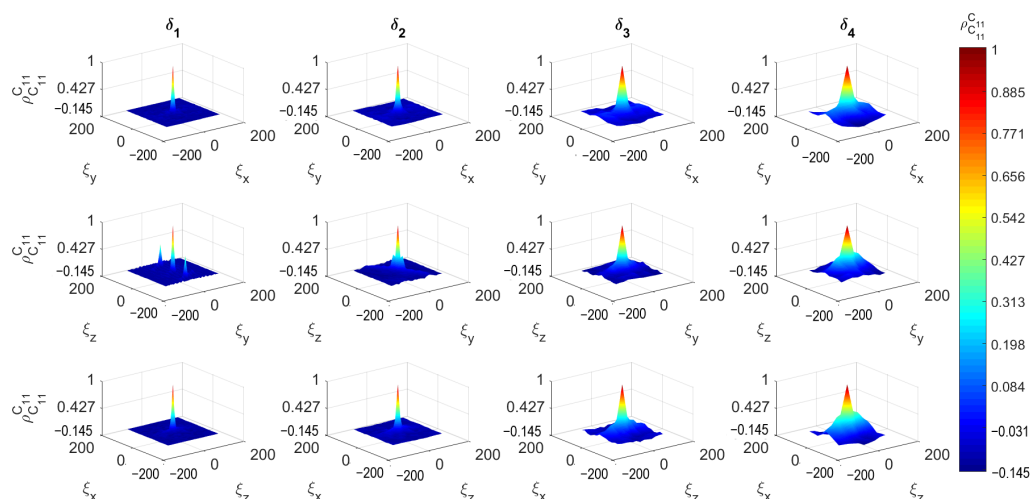


Figure 8. Auto-correlation function of \bar{C}_{11} .

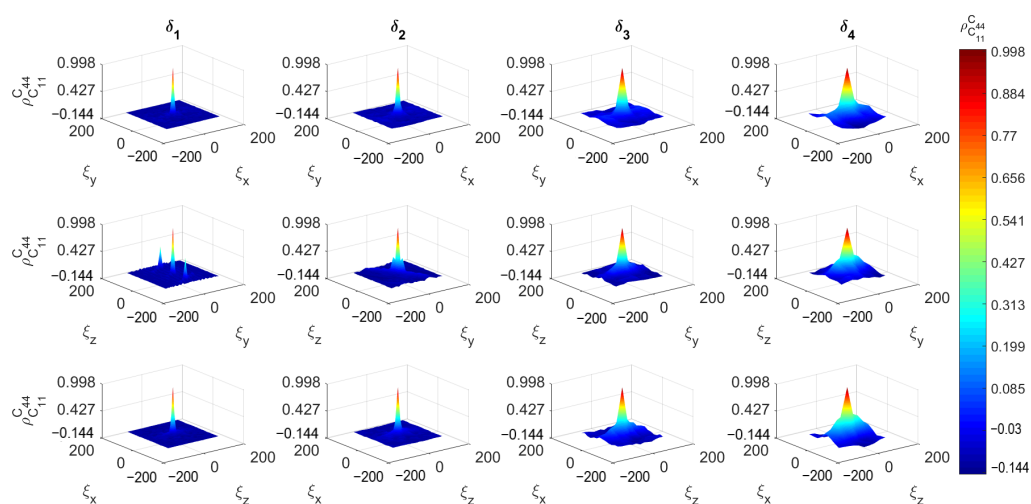


Figure 9. Cross-correlation function between \bar{C}_{11} and \bar{C}_{44} .

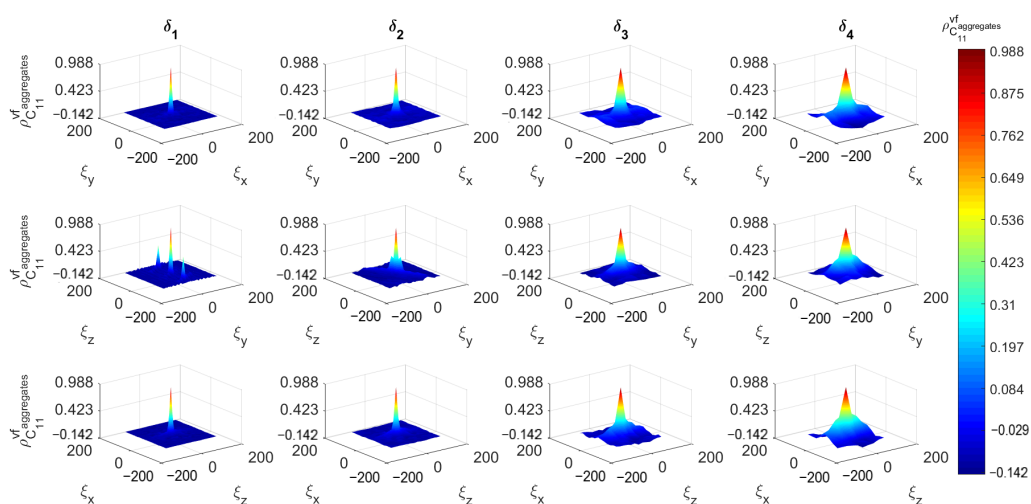


Figure 10. Cross-correlation function between \bar{C}_{11} and vf of aggregates.

Figure 11 presents scatter plots of elasticity components \bar{C}_{11} , \bar{C}_{21} , \bar{C}_{31} , \bar{C}_{44} and vf of aggregates corresponding to data obtained in δ_3 . These plots show that there is a strong positive correlation among all elasticity components and also between the elasticity

components and the vf of aggregates, which verifies the fact that morphological uncertainty in the microstructure of concrete can affect significantly its homogenized properties.

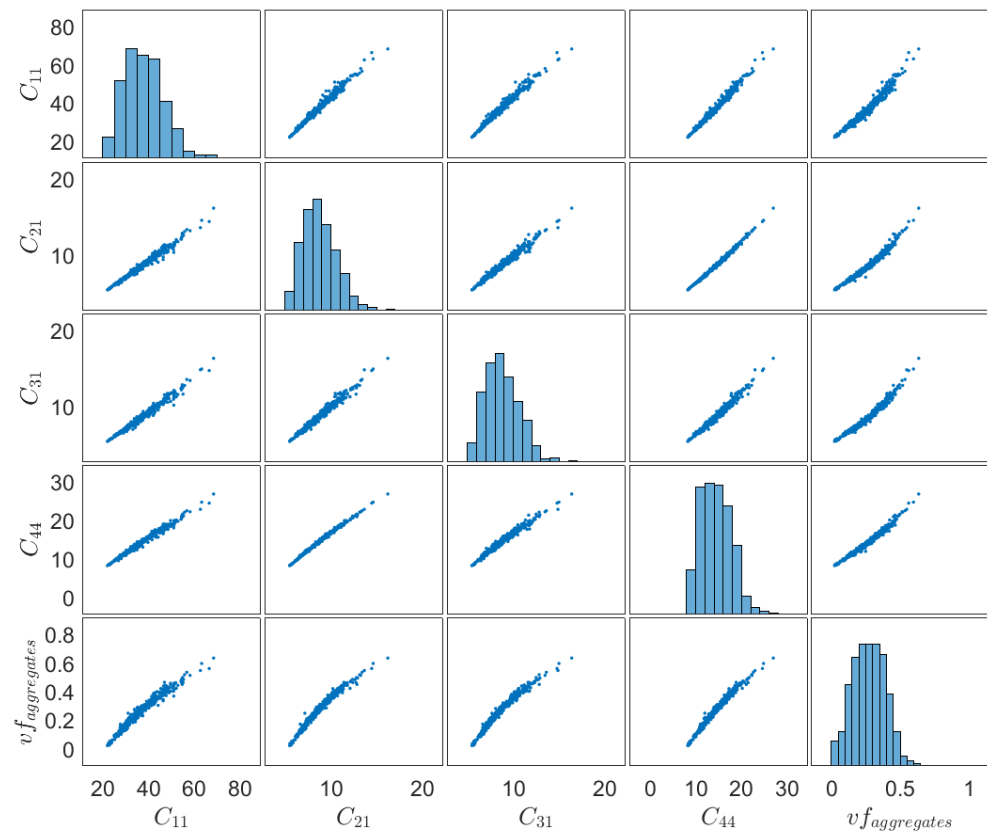


Figure 11. Scatter plots of elasticity components \bar{C}_{11} , \bar{C}_{21} , \bar{C}_{31} , \bar{C}_{44} and vf of aggregates for δ_3 (correspondence of subscripts: 1 \rightarrow 11, 2 \rightarrow 22, 3 \rightarrow 33, 4 \rightarrow 12).

5. Conclusions

- In this paper, the random spatially varying apparent elasticity tensor of 3D concrete microstructures has been computed using CT images of a cubic specimen for the reconstruction of concrete microstructure and computational homogenization.
- A complete probabilistic description of the spatial variation of the elastic properties of concrete has been achieved through computation of the respective mesoscale random fields. In this way, it was possible to assess the effect of randomness in microstructure on the mechanical behavior of concrete based on the statistical characteristics (empirical distribution and correlation functions) of the random fields.
- A moderate to large variability of the local volume fraction of the constituents (pores, cement paste and aggregates) has been observed depending on the scale factor δ considered.
- This was reflected on the moderate to high COV of the apparent axial and shear stiffness, meaning that microstructural uncertainty can lead to substantial random spatial variation of the mechanical properties of concrete.
- The computed random material property fields can be used for the stochastic FE analysis of concrete structures.
- The consideration of the interfacial transition zone (ITZ) between cement paste and aggregates and the determination of random fracture properties could constitute the subject of future research.

Author Contributions: Conceptualization, G.S. and D.S.; methodology, G.S. and D.S.; software, D.S. and P.M.; investigation, P.M.; writing—original draft preparation, G.S., D.S. and P.M.; writing—review and editing, G.S.; visualization, D.S.; supervision, G.S.; funding acquisition, G.S. All authors have read and agreed to the published version of the manuscript.

Funding: This research is co-financed by Greece and the European Union (European Social Fund—ESF) through the Operational Programme “Human Resources Development, Education and Lifelong Learning 2014–2020” in the context of the project “Stochastic multiscale modeling of concrete structures reinforced with graphene nanoparticles—Investigation of the effect of nano-inclusions on the mechanical properties of concrete” (MIS 5047867).



Operational Programme
Human Resources Development,
Education and Lifelong Learning
 Co-financed by Greece and the European Union



Institutional Review Board Statement: Not applicable.

Informed Consent Statement: Not applicable.

Data Availability Statement: The data used in this study are available from the second author (D.S.) upon reasonable request.

Acknowledgments: The authors wish also to acknowledge Magnitiki Patron S.A. [18] for conducting the CT scans on the concrete specimen and providing all the necessary DICOM files in order to accomplish the present research work.

Conflicts of Interest: The authors declare no conflict of interest. The funders had no role in the design of the study; in the collection, analyses, or interpretation of data; in the writing of the manuscript, or in the decision to publish the results.

References

- Hill, R. Elastic properties of reinforced solids: Some theoretical principles. *J. Mech. Phys. Solids* **1963**, *11*, 357–372. [[CrossRef](#)]
- Ostoja-Starzewski, M. Material spatial randomness: From statistical to representative volume element. *Probabilistic Eng. Mech.* **2006**, *21*, 112–132. [[CrossRef](#)]
- Savvas, D.; Stefanou, G.; Papadrakakis, M. Determination of RVE size for random composites with local volume fraction variation. *Comput. Methods Appl. Mech. Eng.* **2016**, *305*, 340–358. [[CrossRef](#)]
- Savvas, D.; Stefanou, G. Determination of random material properties of graphene sheets with different types of defects. *Compos. Part B Eng.* **2018**, *143*, 47–54. [[CrossRef](#)]
- Liu, T.; Qin, S.; Zou, D.; Song, W.; Teng, J. Mesoscopic modeling method of concrete based on statistical analysis of CT images. *Constr. Build. Mater.* **2018**, *192*, 429–441. [[CrossRef](#)]
- Chung, S.Y.; Kim, J.S.; Stephan, D.; Han, T.S. Overview of the use of micro-computed tomography (micro-CT) to investigate the relation between the material characteristics and properties of cement-based materials. *Constr. Build. Mater.* **2019**, *229*, 116843. [[CrossRef](#)]
- Grigoriu, M.; Garboczi, E.; Kafali, C. Spherical harmonic-based random fields for aggregates used in concrete. *Powder Technol.* **2006**, *166*, 123–138. [[CrossRef](#)]
- Huang, J.; Peng, Q. A fast algorithm for multifield representation and multiscale simulation of high-quality 3D stochastic aggregate microstructures by concurrent coupling of stationary Gaussian and fractional Brownian random fields. *Int. J. Numer. Methods Eng.* **2018**, *115*, 328–357. [[CrossRef](#)]
- Constantinides, G.; Ulm, F.J. The effect of two types of CSH on the elasticity of cement-based materials: Results from nanoindentation and micromechanical modeling. *Cem. Concr. Res.* **2004**, *34*, 67–80. [[CrossRef](#)]
- Wriggers, P.; Moftah, S. Mesoscale models for concrete: Homogenisation and damage behaviour. *Finite Elem. Anal. Des.* **2006**, *42*, 623–636. [[CrossRef](#)]
- Huang, Y.; Yan, D.; Yang, Z.; Liu, G. 2D and 3D homogenization and fracture analysis of concrete based on in-situ X-ray Computed Tomography images and Monte Carlo simulations. *Eng. Fract. Mech.* **2016**, *163*, 37–54. [[CrossRef](#)]
- Tal, D.; Fish, J. Stochastic multiscale modeling and simulation framework for concrete. *Cem. Concr. Compos.* **2018**, *90*, 61–81. [[CrossRef](#)]
- Dubey, V.; Noshadravan, A. A probabilistic upscaling of microstructural randomness in modeling mesoscale elastic properties of concrete. *Comput. Struct.* **2020**, *237*, 106272. [[CrossRef](#)]

14. Herman, G.T. *Fundamentals of Computerized Tomography: Image Reconstruction from Projections*; Springer Science & Business Media: New York, NY, USA, 2009.
15. Daigle, M.; Fratta, D.; Wang, L. Ultrasonic and X-ray tomographic imaging of highly contrasting inclusions in concrete specimens. *Site Charact. Model.* **2005**, *GSP 138*, 1–12.
16. Balázs, G.L.; Lubl6y, .; F6ldes, T. Evaluation of concrete elements with X-ray computed tomography. *J. Mater. Civ. Eng.* **2018**, *30*, 06018010. [[CrossRef](#)]
17. Baxter, S.; Hossain, M.I.; Graham, L. Micromechanics based random material property fields for particulate reinforced composites. *Int. J. Solids Struct.* **2001**, *38*, 9209–9220. [[CrossRef](#)]
18. Magnitiki Patron S.A. Available online: <https://www.magnitikipatron.com> (accessed on 15 February 2021).
19. RadiAnt DICOM Viewer. Available online: <https://www.radiantviewer.com> (accessed on 15 February 2021).
20. Hashin, Z. Analysis of composite materials: A survey. *J. Appl. Mech.* **1983**, *50*, 481–505. [[CrossRef](#)]
21. Chwa, M.; Muc, A. Design of reinforcement in nano- and microcomposites. *Materials* **2019**, *12*, 1474. [[CrossRef](#)]
22. Kanit, T.; Forest, S.; Galliet, I.; Mounoury, V.; Jeulin, D. Determination of the size of the representative volume element for random composites: statistical and numerical approach. *Int. J. Solids Struct.* **2003**, *40*, 3647–3679. [[CrossRef](#)]
23. Zeman, J.; Sejnoha, M. From random microstructures to representative volume elements. *Model. Simul. Mater. Sci. Eng.* **2007**, *15*, 325–335. [[CrossRef](#)]
24. Zohdi, T.I.; Wriggers, P. *An Introduction to Computational Micromechanics*, 2nd ed.; Lecture Notes in Applied and Computational Mechanics; Springer: Heidelberg, Germany, 2008; Volume 20.
25. Wimmer, J.; Stier, B.; Simon, J.W.; Reese, S. Computational homogenisation from a 3D finite element model of asphalt concrete—linear elastic computations. *Finite Elem. Anal. Des.* **2016**, *110*, 43–57. [[CrossRef](#)]
26. Savvas, D.; Stefanou, G.; Papadopoulos, V.; Papadrakakis, M. Effect of waviness and orientation of carbon nanotubes on random apparent material properties and RVE size of CNT reinforced composites. *Compos. Struct.* **2016**, *152*, 870–882. [[CrossRef](#)]
27. Reccia, E.; De Bellis, M.L.; Trovalusci, P.; Masiani, R. Sensitivity to material contrast in homogenization of random particle composites as micropolar continua. *Compos. Part Eng.* **2018**, *136*, 39–45. [[CrossRef](#)]
28. Hazanov, S.; Huet, C. Order relationships for boundary conditions effect in heterogeneous bodies smaller than the representative volume. *J. Mech. Phys. Solids* **1994**, *42*, 1995–2011. [[CrossRef](#)]
29. Miehe, C.; Koch, A. Computational micro-to-macro transitions of discretized microstructures undergoing small strains. *Arch. Appl. Mech.* **2002**, *72*, 300–317. [[CrossRef](#)]
30. Stefanou, G. The stochastic finite element method: Past, present and future. *Comput. Methods Appl. Mech. Eng.* **2009**, *198*, 1031–1051. [[CrossRef](#)]